Chinese Journal of Chemical Engineering 67 (2024) 206–219

Contents lists available at ScienceDirect

Chinese Journal of Chemical Engineering

journal homepage: www.elsevier.com/locate/CJChE

Review

Rate-limiting factors in hydrate decomposition through depressurization across various scales: A mini-review

Xian Sun [1, #], Peng Xiao [1, #], Qinfeng Shi [2], Lingban Wang [1], Zhenbin Xu [1], Yuhao Bu [1], Xiaohui Wang [1], Yifei Sun [1], Changyu Sun [1, *], Guangjin Chen [1, *]

[1] State Key Laboratory of Heavy Oil Processing, China University of Petroleum (Beijing), Beijing 102249, China
[2] Jining University, Jining 273115, China

ARTICLE INFO

Article history:
Received 28 June 2023
Received in revised form
25 October 2023
Accepted 30 October 2023
Available online 5 December 2023

Keywords:
Gas hydrate
Rate-limiting factors
Research scale
Depressurization
Decomposition

ABSTRACT

Natural gas hydrate is an energy resource for methane that has a carbon quantity twice more than all traditional fossil fuels combined. However, their practical application in the field has been limited due to the challenges of long-term preparation, high costs and associated risks. Experimental studies, on the other hand, offer a safe and cost-effective means of exploring the mechanisms of hydrate dissociation and optimizing exploitation conditions. Gas hydrate decomposition is a complicated process along with intrinsic kinetics, mass transfer and heat transfer, which are the influencing factors for hydrate decomposition rate. The identification of the rate-limiting factor for hydrate dissociation during depressurization varies with the scale of the reservoir, making it challenging to extrapolate findings from laboratory experiments to the actual exploitation. This review aims to summarize current knowledge of investigations on hydrate decomposition on the subject of the research scale (core scale, middle scale, large scale and field tests) and to analyze determining factors for decomposition rate, considering the various research scales and their associated influencing factors.

1. Introduction

Natural gas hydrates (NGHs) are widely distributed in continental margins and permafrost zones [1]. Due to the huge resource potential, NGHs have received extensive attention as a potential alternative energy. Several methods have been carried out based on the principle of destructing the stability situations of NGHs systems for fluid extraction [2], which includes depressurization [3–5], inhibitor injection [6–8], thermal stimulation [9–11], carbon dioxide replacement [12–14], and combinations of these methods [15,16]. Among these methods, depressurization is regarded as the most effective and commercially feasible one for NGHs exploitation because of its low external energy input, low cost, and simple operation; It thereby attracts extensive attention from relevant scholars [3,17–19]. Field production tests in Mallik [20], Nankai Trough [21], and the Shenhu area [22] have proved the technical feasibility of the depressurization method for gas hydrate development [23]. However, only limited field tests have been carried out in nature so far because it needs long-time preparation and huge cost, and it is hard to conduct [24]. Therefore, experimental investigations play a significant role in developing the exploitation technologies for NGHs and clarifying the corresponding mechanisms [25]. Over the past several decades, numerous research have devoted to studying the methane hydrate decomposition behavior, and the focus shifted from the fundamental research of hydrate decomposition mechanism to the selection and optimization of the hydrate development methods. The field application of laboratory data is of great significance to the NGHs economical exploitation. However, the scale of the reservoir significantly influences depressurization-induced gas production, leading to variations in hydrate dissociation behaviors observed in the experimental studies compared to field tests. Hydrate dissociation process is essentially a multiphase–multicomponent heat and mass transfer problem coupled with intrinsic kinetics [26,27], all of them are the factors influencing on the hydrate decomposition rate. The intrinsic kinetics of hydrate decomposition characterizes the process of hydrate material transformation under the condition of excluding the influence of mass transfer and heat

* Corresponding authors.
E-mail addresses: cysun@cup.edu.cn (C. Sun), gjchen@cup.edu.cn (G. Chen).
# These authors contributed equally to this work.

https://doi.org/10.1016/j.cjche.2023.10.014
1004-9541/

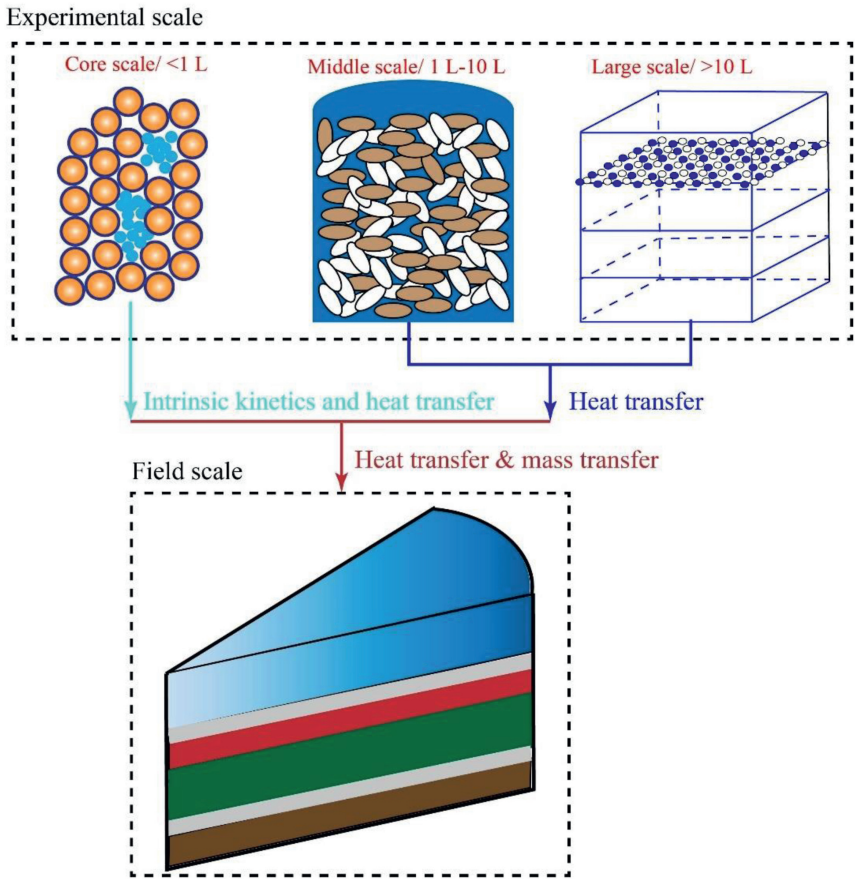

Fig. 1. Schematics illustrating the rate-limiting factors of various research studies.

transfer. The determining factor of gas production depends on the reservoir scale [15]. The determining factor for the core-scale cases is the intrinsic kinetics of hydrate decomposition [28]. This implies that the dissociation rate model for core-scale cases can be formulated as a function of intrinsic kinetics, as discussed in the study by Kim *et al.* [29], and the hydrate dissociation rate in core-scale studies can be viewed as being limited by intrinsic kinetics. However, for field-scale tests, heat and mass transfer are the dominant factors, and intrinsic kinetics can be negligible [28,30] (see in Fig. 1).

In recent years, there has been a notable advancement in the development of experimental apparatus, which has expanded from core-scale setups to encompass larger-scale configurations aimed at stimulating real exploitation conditions [15,31]. In Fig. 2, experimental studies with the research topics "depressurization" and "natural gas/methane hydrate" on depressurization-induced hydrate production from 2002 to 2020 are summarized and classified by research scale. Chong *et al.* [18] gives boundaries of middle-scale and large-scale reactors (1–10 L for middle-scale and >10 L for large-scale, respectively). In addition, the core scale is known as the centimeter scale. The largest volume of the centimeter scale is 1 L (the length, width and height of the reactor are all 10 cm). Thus, to facilitate the understanding and summary, the core, middle, and large research scale refer to the volume of the apparatus used for gas hydrate decomposition experiments is 0–1 L, 1–10 L and >10 L, respectively in this work. As seen in Fig. 2, experimental studies still concentrated on core- and middle-scale. Moreover, as mentioned below, large-scale tests are insufficient to replace field tests. Moreover, in most cases, the findings obtained at these various scales are directly utilized for mutual comparison and verification. This hinders the transition from experimental results to industrial production. This work aims to summarize the existing knowledge of investigations on hydrate decomposition on the subject of the research scale (core scale, middle scale, large scale and field tests) and to analyze determining factors for hydrate decomposition with various research scale as well as their related influencing factors.

2. Hydrate Decomposition *via* Depressurization With Different Research Scales

To facilitate the follow-up discussion, the process of hydrate decomposition *via* depressurization was divided into three periods: (i) free gas release, (ii) mixed gas (*i.e.*, both free gas and hydrate dissociation gas) release, and (iii) hydrate dissociation gas release [4,46]. Compared with the stage (iii), the durations of stages (i) and (ii) are much shorter. Relevant scholars combined stages (i) and (ii) into the depressurizing period (DP), and stage (iii) was called the steady/constant pressure period (CP) [61].

2.1. Core-scale research

2.1.1. Rate-limiting factors

The decomposition intrinsic dynamics is considered as the determining factor for gas production in core-scale tests [15,28,136,137]. Kim *et al.* [29] derived an apparent dissociation rate based on an intrinsic model for the kinetics of hydrate decomposition and determined the rate constant from experimental data. This result has been confirmed and extended in later studies [15,28,136].

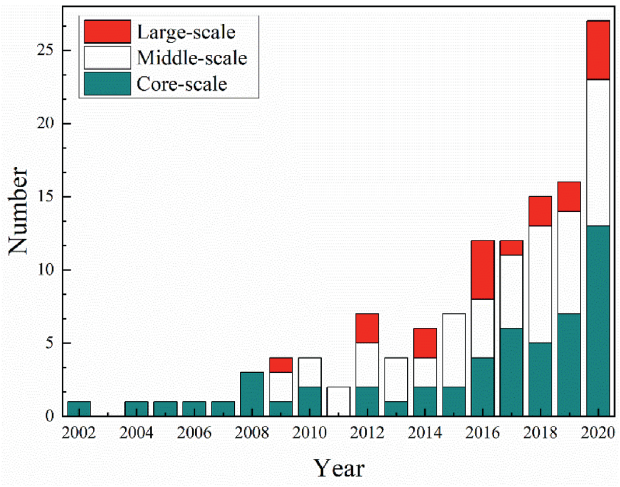

(a)

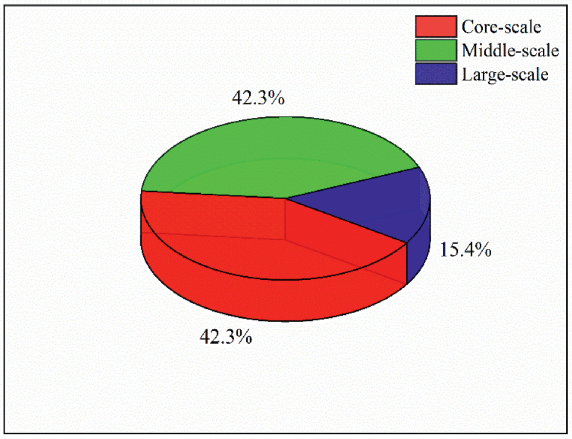

(b)

Fig. 2. (a) Summary of the scale of hydrate devices used for depressurization-induced hydrate decomposition over the past two decades [2–5,17–19,23–26,28,30,32–135]; (b) research scale distribution of publications.

Based on it, Tang *et al.* [28] conducted sensitivity analyses and provided compelling evidence that hydrate dissociation kinetics significantly impact gas production behavior in hydrate-bearing cores. Yet, Oyama *et al.* [37] argued that the heat transferred from the ambient is predominant for hydrate dissociation during the stage (iii). By comparing the methane hydrate decomposition rate under the limitation of intrinsic kinetics, heat transfer, and mass transfer separately, Hong *et al.* [138] proved that the degree of the limiting factors was affected by the reaction time. Their findings demonstrated that the extent of these limiting factors was influenced by the progression of the reaction over time. Initially, due to rapid heat transfer, intrinsic kinetics emerged as the dominant factor. However, as the sensible heat was depleted, heat transfer from the boundaries assumed the role of the rate-limiting factor. Overall, rate-limiting factors of depressurization-induced hydrate decomposition are intrinsic kinetics [28,136,139] and heat transfer [37] in a core-scale reactor.

According to the solution method, kinetics models used for describing the hydrate decomposition process include theoretical, numerical, and analytical models [140]. Of these factors, the theoretical model is purely derived based on the basic theory and gives the physical and mathematical relationships between the relevant variables of the hydrate dissociation process without any semi-empirical correlation. In the study by Oyama *et al.* [37], a theoretical model was employed to describe the overall dissociation rate as the combined effect of both forward and backward reaction rates. Moreover, the decomposition process of methane hydrate was also modeled as a first-order reaction, so as to obtain another expression for the hydrate decomposition rate. Compared with two equations of the overall dissociation rate, the authors figured out the overall hydrate dissociation coefficient. The physical and mathematical relations between the related variables are only derived from the basic theory of chemical engineering. However, due to the complexity of the actual chemical process and many influencing factors, the theoretical model obtained by Oyama *et al.* [37] was under following assumptions: (a) neglecting the formation of ice; (b) The core temperature equals the three phase equilibrium temperature of the corresponding pressure with continuous gas production at the production pressure; (c) A gas flow path is generated during the initial depressurization process.

In contrast, the numerical method refers to the calculation aiming at obtaining numerical results. The numerical analysis brings huge computational costs, and the efficiency and accuracy of numerical calculation often depend on the calculation tools. Therefore, in early research, the use of numerical calculation was obviously limited. With the progress of scientific computing, the efficiency of solving equations has been dramatically improved, which makes the numerical solution the most widely used method in recent years. The simulator of transport of unsaturated groundwater and heat (TOUGH)-Fx/hydrate has been adopted to discuss hydrate decomposition [28,139], which belongs to the TOUGH family simulation code and is the most widely used reservoir model applied for the NGHs production evaluation. Software of the computational fluid dynamic was also widely used in hydrate decomposition research [141–143].

The analytical method involves expressing all relationships among model parameters, initial conditions, input information, simulation time, and results through closed-form solutions of differential equations [140]. This approach is widely utilized in hydrate decomposition research, as seen in previous studies [29,138,144]. For example, Hong *et al.* [138] reported an analytical model of methane hydrate decomposition rate under the limitation of intrinsic kinetics, heat transfer, and mass transfer, respectively. The results proved that the degree of the limiting factors was affected by the reaction time. Due to the rapid heat transfer rate, intrinsic kinetics is the rate-controlling factor early. Then, heat transferred from boundaries becomes the rate-limiting factor after the sensible heat is exhausted.

2.1.2. *Influence of the research volume*

Indeed, the rate-limiting factors in hydrate decomposition do not abruptly transition at a specific scale but instead exhibit a gradual shift. According to the obtained mathematical model, for core-scale cases, the limitation of intrinsic kinetics gradually weakened with the increase of the research volume, while that of heat transfer was aggravated. To exclude the other effects and investigate the intrinsic kinetics of hydrate dissociation alone, Kim *et al.* [29] adopted a sufficient stirring speed and maintained the system at a constant temperature during the hydrate dissolution process. A kinetic model of hydrate dissociation rate that only considered the limiting effect of the intrinsic kinetics was given to describe the experimental data.

$$-\frac{\mathrm{d}n_{\mathrm{H}}}{\mathrm{d}t}=k_{\mathrm{d}}a_{\mathrm{dec}}\left(f_{\mathrm{se}}-f_{\mathrm{g}}\right) \tag{1}$$

where n_H is the total moles of methane contained in the hydrate particles; k_d is the rate constant of intrinsic decomposition; a_{dec} denotes the decomposing area of methane hydrate particles; f_{se}, f_g represent the fugacity of methane corresponding to the three-phase equilibrium state and decomposition pressure, respectively. In Eq. (1), k_d is affected by temperature and activation energy, and the formulation is expressed as:

$$k_d = k_d^0 e^{-\Delta E/RT} \tag{2}$$

where ΔE represents the activation energy, $J \cdot mol^{-1} \cdot K^{-2}$; R is gas constant, 8.314 $J \cdot mol^{-1} \cdot K^{-1}$; T is the temperature of the system, K; k_d^0 presents the intrinsic kinetics constant. The kinetics model can also be correlated with hydrate reservoir volume, and the expression can be rewritten as below. Similar discussions have also been proposed by another scholar [145].

$$-\frac{dn_H}{dt} = k_d^0 e^{-\Delta E/RT} A_{dec} V (P_{se} - P_g) \tag{3}$$

where A_{dec} represents the decomposition area per unit volume, m^{-1}; V is the volume of the hydrate reservoir, m^3.

$$A_{dec} = A_{HS} \phi S_H \tag{4}$$

where A_{HS} is the surface area of 1 m^3 NGHs, $A_{HS} = 3.75 \times 10^5$ $m^2 \cdot m^{-3}$ [146]; ϕ is the porosity; S_H presents hydrate saturation.

According to Eq. (4), A_{dec} does not change with the research volume. Consequently, when solely taking into account the constraint imposed by intrinsic kinetics, it becomes evident that with larger research volume, the rate of hydrate decomposition tends to increase. Moreover, the limiting effect of intrinsic kinetics diminishes as the research volume expands. This implies that intrinsic kinetics exerts a less restriction on the rate of methane hydrate decomposition when employing a large-scale volume.

As for the heat transfer limitation, an analytical solution for the transfer velocity of the methane hydrate dissociation interface [138] was presented with the following correlation.

$$\frac{dX(t)}{dt} = \lambda \sqrt{\frac{\alpha}{t}} \tag{5}$$

where $X(t)$ is the hydrate interface location, α is thermal diffusivity, and λ is the eigenvalue. As shown in Eq. (5), the transfer position of methane hydrate decomposition surface per unit time is independent of the reservoir volume under the condition of being limited by heat transfer only. However, it is important to recognize that in larger volume settings, the process necessitates more time for transfer, resulting in a more prolonged influence of the heat transfer process. In summary, as the research volume enlarges, the degree of limitation attributed to decomposition kinetics diminishes, while the impact of heat transfer becomes more pronounced, as visually depicted in Fig. 3.

This view was confirmed in the research of Chen and Hartman [147], in which an analytical solution was obtained, and the derivation method was similar to that of Hong *et al.* [138]. In the work by Chen and Hartman [147], the roles of heat transfer and intrinsic kinetics were evaluated by considering the contribution fraction of each process. As seen in Eq. (6), w_h and w_i are contribution fractions of heat transfer and intrinsic kinetics, respectively. Both of them are dimensionless quantities. Notably, w_h and w_i were not computed independently; Instead, the ratio of both quantities was treated as a unified entity. In addition, both w_h and w_i are transient processes, functions of time, the initial methane hydrate thickness, and the temperature difference between the system and the phase

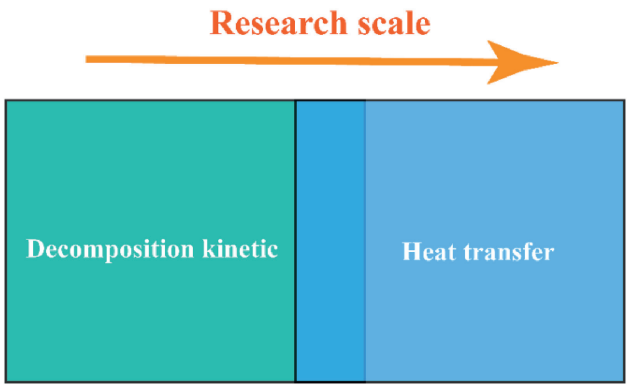

Fig. 3. The shift between the rate-limiting factors of intrinsic kinetics and heat transfer with scale increases.

boundary. Thus, the ratio of the contribution fraction of each process was estimated by Eq. (6) in Chen and Hartman's [147] work.

$$\frac{w_h}{w_i} = l \cdot [1 - \exp(-k_d t)] \cdot \sqrt{\frac{\rho_H \Delta h}{2kt\Delta T}} \tag{6}$$

where l is the initial thickness of the methane hydrate on the wall. k is the thermal conductivity of dissociated hydrate, ρ_H is the density of the hydrate, Δh is the enthalpy of methane hydrate dissociation (436.5 $kJ \cdot kg^{-1}$), and ΔT represents the temperature difference between initial temperature and phase equilibrium temperature, respectively.

Besides the research volume, various other factors also exert influence on the rate-limiting factors in core-scale hydrate decomposition. Specifically, concerning hydrate decomposition kinetics, as indicated by Eq. (3), factors such as the initial system temperature, pressure differential, and particle surface area play pivotal roles in altering the extent to which intrinsic kinetics act as the limiting factor, thereby affecting the rate of methane hydrate decomposition. In the realm of heat transfer, the influencing factors encompass the initial temperature, initial water saturation, and production pressure. Overall, there is an overlap in the factors that influence both intrinsic kinetics and heat transfer.

2.2. Large-scale research

2.2.1. Rate-controlling factors

In recent studies, laboratory equipment has undergone a transformation from core-scale setups to larger-scale configurations, allowing for more realistic simulations of hydrate dissociation behaviors akin to those found in actual NGH reservoirs [69]. As of now, China [79,109,148], Germany [149], the United States of America [40], and Japan [56] have developed several large-scale simulators and carried out a series of studies on methane hydrate dissociation using different methods. However, most large-scale experimental studies fail to identify the limiting effect of mass transfer on the decomposition rate of hydrate [4,49,109,150,151], including the study of depressurization-induced hydrate decomposition with a 1710-L device [56].

Some simulation studies with a larger research scale pointed out that mass transfer plays a more important limitation role during the hydrate dissociation process [152,153]. However, it is crucial to acknowledge that the extensive research scales employed in simulations are often challenging to replicate in experimental settings. Thus, heat transfer is the main rate-limiting factor of the hydrate decomposition rate in a large-scale experimental study. The decomposition of methane hydrate involves heat sources such as the sensible heat stored within the undecomposed hydrate deposit and

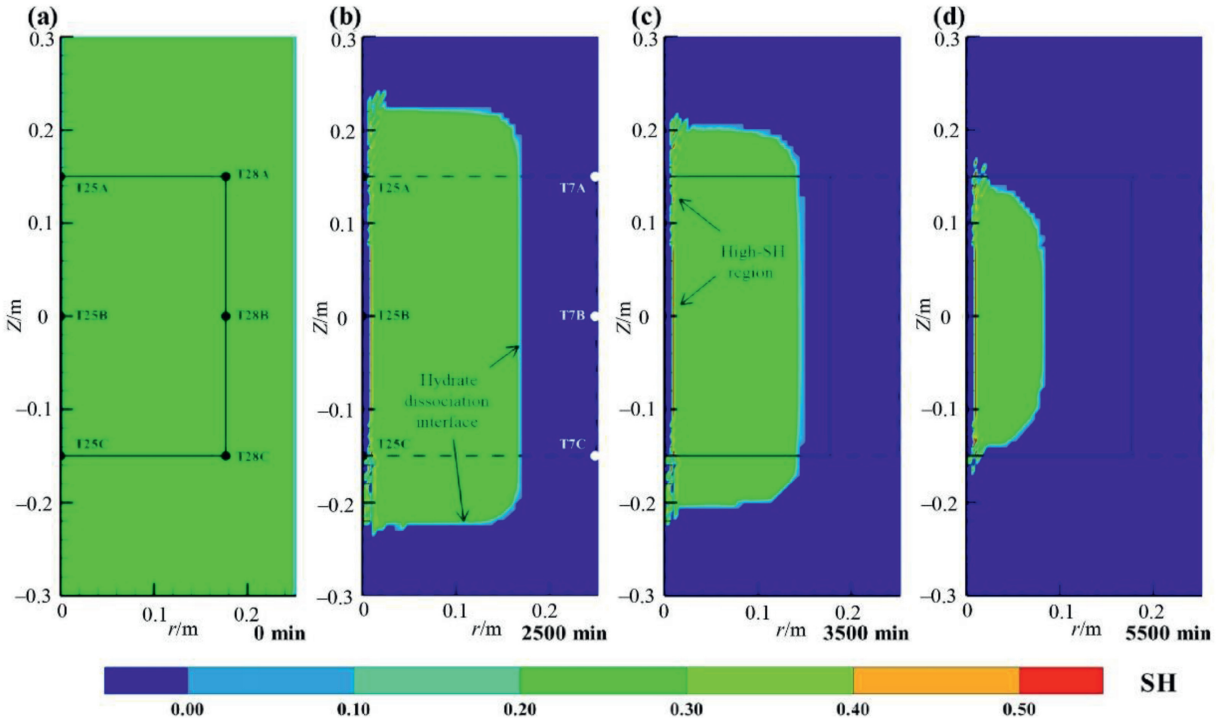

Fig. 4. Evolution of the spatial distribution of hydrate saturation over time of numerical simulation results during hydrate dissociation [49].

heat conducted from the surrounding environment. Methane gas recovery curves obtained by Kou *et al.* [105] show little discrepancy under different boundary conditions during the DP process. However, during the CP stage, gas production behavior was distinctly different under the condition of isothermal and semi-adiabatic boundaries. This is to say, the latent heat is exhausted first (corresponding to stage (ii)) and then is the environmental heat conducted from the device boundaries (stage (iii)) [4,15]. In other words, the heat conducted from the external environment has little impact on the DP stage but plays a vital role during the CP stage. The gas production rate depended on the CP stage [4,55,109]. In view that the heat conducted from the external surroundings is the main driving force for the CP stage, it is also the dominate limiting factor affecting the whole hydrate decomposition process [4,15,49,50,55,105]. A simulation of the

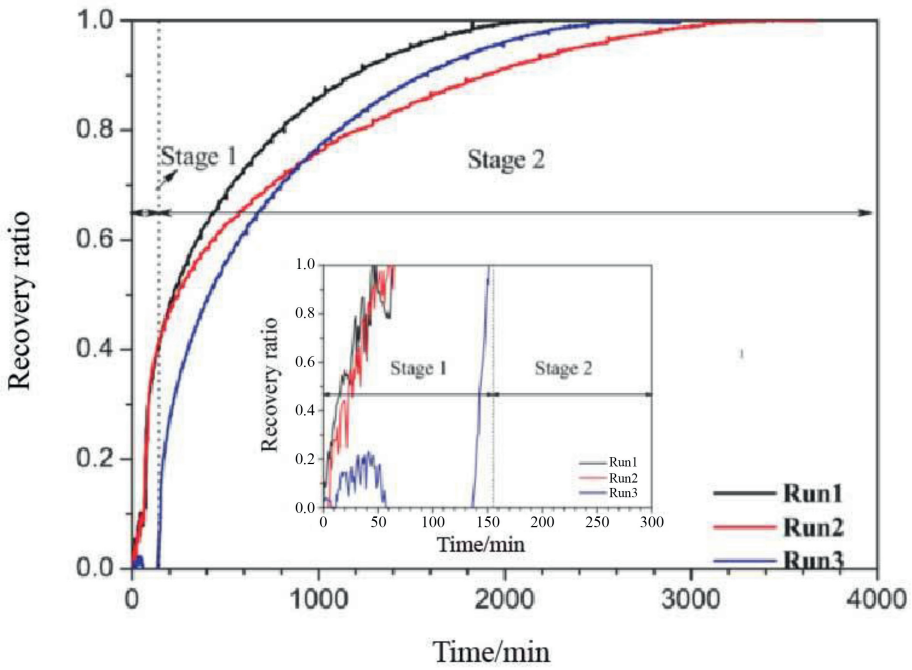

Fig. 5. Curves of recovery ratios during hydrate dissociation for Runs 1–3 and the partial enlargement of the first 300 min during hydrate dissociation [49].

hydrate dissociation process [49] has shown that the direction of the methane hydrate dissociation front aligns with the external heat transfer, with both progressing inward from the reactor boundaries towards the center [55], as illustrated in Fig. 4.

Fig. 5 shows the curves of recovery ratios during hydrate dissociation for Runs 1–3 [49]. Whereas, Runs 1–3 were performed with the isothermal-, semi-adiabatic- and adiabatic-boundary, respectively. As observed, in the CP stage, Run 1, conducted under isothermal conditions, exhibited a significantly more rapid increase in gas production rate compared to Run 2, which employed a semi-adiabatic boundary. As mentioned above, heat conduction from the ambient is the dominant driving force of hydrate dissociation. Thus, the isothermal boundary condition promotes the dissociation of gas hydrate as compared with the semi-adiabatic boundary. When comparing Run 1 to Run 3, it is apparent that the production rate in the early CP stage of Run 1 surpasses that in Run 3, while the production rate in the later phase of the CP stage in Run 1 appears to lag behind Run 3. However, the overall characteristics of gas production rates in Run 1 and Run 3 are similar. Because of the different distributions of wellbore, the flow direction of Run 1 is identical to the heat transfer direction, while the flow direction of Run 3 is opposite to the heat transfer direction. One might expect that these different convection directions would result in a faster heat transfer rate in Run 1 than Run 3. However, the experimental result suggests that the influence of hydrate convection on heat dissociation in the CP stage may not be obvious.

The transfer direction of hydrate decomposition front for actual field-scale tests is opposite to the large-scale experimental studies. For field-scale tests, the NGHs decomposition front starts from the exploitation well and then transmits to the surrounding area [154]. The real NGHs reservoir environment is generally characterized by low permeability, and the NGHs decomposition process is significantly restricted by mass transfer [28]. In addition, the real NGHs environment also has a different thermodynamic condition [155]. Recently, relevant scholars have introduced a novel criterion for identifying rate-limiting factors, relying on the characteristics of the dissociation front advance. The advance curve of the hydrate decomposition front may be a non-piston-like mode [47] when the hydrate dissociation was carried out under a constant-temperature boundary. For the adiabatic-thermal boundary, it may be in a piston-like dissociation mode [55,139]. In addition to the thermal boundary conditions, the initial permeability of the hydrate deposit and internal reaction rate influence the hydrate decomposition front mode [156–159].

Moreover, considering that the initial permeability, thermal boundary conditions, and intrinsic reaction rate serve as indicators of mass transfer, heat transfer, and intrinsic kinetics limitations, respectively [31,138,140,160–162], the determination of rate-limiting factors hinges on the dissociation front characteristics within the targeted NGHs reservoirs.

2.2.2. Influencing parameters of the hydrate decomposition rate

In a large-scale reactor, the primary rate-limiting factor affecting the hydrate decomposition rate is heat transfer. This rate is influenced by two main heat sources: the sensible heat contained within the undecomposed hydrate deposit and the heat conducted from the external environment. Consequently, the parameters associated with these two heat transfer processes also have a significant impact on the rate of hydrate decomposition.

(1) Initial water saturation

The initial water saturation exerts a significant influence on the thermal properties of the hydrate sediment, notably altering its heat capacity and thermal conductivity, thereby impacting the heat transfer process. In cases of gas saturation, the duration of the DP stage was much shorter than that of the water-saturated case under identical pressure reduction conditions. This is because more free gas exists in the gas-saturated system, which has a faster exhaust rate than the water displacement [153]. However, hydrate decomposition during the DP period depends on the latent heat; more latent heat will be provided in case of high-water content. This leads to more hydrate decomposition in this stage. A relevant study showed that 87% of methane hydrate was decomposed in 41 min during the DP stage in a water-saturated environment, whereas in a water saturated environment, 85% of methane hydrate was decomposed over an extended period of 65 min [163]. The hydrate decomposition quantity is larger, and the methane hydrate decomposition speed is faster during the DP stage in the water-saturated case. However, during the CP stage, there exist opposite conclusions [164]. The external heat transfer rate is slower in a water-saturated environment. The curve of temperature changing with time was “L-shaped” in the water-saturated hydrate reservoir. In contrast, for the gas-saturated hydrate reservoir, the temperature variation with time was “V-shaped” [164]. As aforesaid, in the process of hydrate dissociation, the sensible heat was first exhausted, and the environmental heat was conducted from the device boundaries.

(2) Initial reservoir temperature

The mass of the methane hydrate dissociated is related to the sensible heat consumption during the DP stage [15], a relationship that is proportional to the drop in reservoir temperature. The methane hydrate decomposition mass can be mathematically expressed as below [69].

$$m_{\mathrm{dissDP}} = f\left(T_{\mathrm{res}} - T_{\mathrm{eq}}\right) \tag{7}$$

where m_{dissDP} is the mass of methane hydrate dissociation during the DP stage; T_{res} is the initial hydrate reservoir temperature; And T_{eq} is the hydrate equilibrium temperature corresponding to the production pressure.

Maintaining a constant production pressure, it becomes evident that a lower initial system temperature results in a reduced contribution of sensible heat originating from the reservoir. Thus, a lower production pressure is associated with a diminished rate of hydrate decomposition and a smaller quantity of hydrate decomposition occurring during the DP stage. In addition, a lower initial system temperature also induces a slower gas production rate during the CP stage. This is caused by the low temperature drop and resulted from the small temperature difference between the device and its surroundings [69].

(3) Production pressure

The dissociation behavior of methane hydrate differs significantly depending on whether the production pressure is above or below the quadruple point. If the production pressure is above the quadruple point, hydrate dissociates into water and methane gas. As the production pressure decreases, the pressure drop in the DP stage becomes extensive, which results in the release of more latent heat from the methane hydrate reservoirs. This accelerates the hydrate decomposition rate during the DP stage. For the CP stage, a lower production pressure induces a more substantial temperature difference between the internal and external environments of the system, creating a larger driving force for hydrate decomposition. Li *et al.* [55] discussed the hydrate decomposition behaviors with the production pressures of 4.70, 4.20 and

3.70 MPa, respectively. The results showed that the duration of methane hydrate decomposition during the DP stage ranged from 128.2 min to 42.0 min, with corresponding decomposition rates varying from 18.93 to 88.51 $g \cdot min^{-1}$ across different production pressures. In contrast, during the CP stage, the methane hydrate decomposition times spanned from 8160 min to 3366 min, and the decomposition rates ranged from 2.282 to 5.422 $g \cdot min^{-1}$, again contingent on the specific production pressure conditions. The hydrate decomposition rates of the DP and CP stages were greatly accelerated when the production pressure decreased. Similar findings were also reported in another study with production pressures of 4.8 and 2.5 MPa [68]. In addition, methane hydrate decomposition is more dependent on latent heat with a lower production pressure.

Methane hydrate dissociates into methane gas and ice below the quadruple point, creating a complex scenario. During the DP stage, the available latent heat within the hydrate sediment surpasses that of hydrate decomposition above the quadruple point. In addition, the transformation of pore water into ice would also release heat. Thus, the hydrate decomposition below the quadruple point obviously promotes the heat transfer process during the DP stage. However, for the CP stage, the generated ice weakened the effect of the external heat transfer. Consequently, in this scenario, the dissociation of hydrates relies more heavily on the latent heat contained within the hydrate reservoir.

Moreover, the effects of initial temperature and water saturation on the rate-controlling factors in the above discussion would differ when the production pressure is below the quadruple point [68]. Regarding the impact of water saturation, it was pointed out that the methane hydrate decomposition speed is faster during the DP stage in a water-saturated environment. However, for hydrate production below the quadruple point, the gas production rate is faster from the quadruple point to the production pressure for the gas saturated case. This observation may be attributed to the increased ease of freezing in a gas-saturated environment. In terms of the influence of the initial temperature on the hydrate decomposition, it was emphasized that higher initial temperatures enhance the hydrate decomposition rate in both the DP and CP stages [69]. However, a lower initial temperature will accelerate the methane hydrate decomposition because water is easier to convert to ice when the production pressure is below the quadruple point.

2.3. Middle-scale research

2.3.1. Rate-limiting factors and Stefan number

The main rate-limiting factor of middle-scale depressurization-induced hydrate decomposition is heat transfer [3]. Moreover, latent heat is consumed during the DP stage, and then the heat conducted from the outside environment in the CP stage. In the study of Zhao *et al.* [3], quartz sand, corundum, and silicon carbide were adopted to simulate actual reservoirs, of which the heat capacities and thermal conductivities were 742, 775 and 673 $W \cdot m^{-1} \cdot K^{-1}$; 1.35, 28.82 and 41.90 $J \cdot kg^{-1} \cdot K^{-1}$, respectively. The similar heat capacities of the three kinds of media indicated the same latent heat of hydrate deposits in the three systems. The difference in thermal conductivity between the three kinds of media led to an obvious difference in thermal conductivity behavior among the three systems. According to the results, the internal and external temperature changes of the device were the same for three types of fillers during the DP stage, while those during the CP stage were significantly different. Specifically, in the CP stage, the internal reactor temperature had a sharp increase for the quartz sand case, which was higher than the external environment. The thermal conductivity of quartz sand was smaller than the other two sediments, and the external environment heat cannot be introduced timely, resulting in methane hydrate regeneration and temperature rise.

The Stefan number is introduced to quantitatively evaluate the relationship between the contributions of heat conducted from outside and latent heat on the hydrate decomposition. Stefan number (*Ste*) is defined as the ratio of the sensible heat of the hydrate-bearing sediment to the total consumption heat of methane hydrate decomposition [145]:

$$Ste = \frac{C_p \Delta T}{\phi \Delta H} \cdot \frac{\rho}{\rho_H} \tag{8}$$

where C_p is the hydrate sediment specific heat capacity, ρ is sediment density, and the subscript H represents methane hydrate. $\Delta H(T)$ is the latent heat of methane hydrate dissociation per mole, which is related to the temperature [3,165].

According to Eq. (8), the Stefan number is independent of the reactor volume. In simpler terms, for middle-scale cases, the heat conducted from outside also accounts for the central part of the consumption. Moreover, the proportion is the same as that of the large-scale case. However, this does not mean that the heat transfer characteristics of the depressurization-induced large- and middle-scale methane hydrate dissociation process are identical. Irreversible energy loss is not considered in the above discussions, which varies with the research scales [82]. In addition, during the hydrate decomposition process, factors such as the distance of external heat transfer and the shape of the heat exchange surface would also be affected by the research scale. Consequently, these variations may lead to differing degrees of limitation in the heat transfer process.

2.3.2. Scaling criterion

Li *et al.* [4] studied gas production behavior by depressurization in a large-scale (117.8 L) device and compared it with that obtained from a middle-scale (5.8 L) reactor. Results suggested that the gas production process including (i) free gas release stage, (ii) mixed gas release stage, and (iii) dissociated gas release stage. In addition, period (i) plus period (ii), corresponding to the DP stage, lasted 40 and 36.5 min for the middle- and large-scale reactors, respectively. In contrast, the duration of the CP stage for middle- and large-scale reactors were 300 and 6081 min, respectively. This result illustrates that the research scale has little influence on the duration of the DP stage but has a pronounced impact on the CP stage. The course of the CP stage is significantly longer under large-scale conditions. Therefore, for a large-scale case, hydrate decomposition is restricted by external heat transfer for a longer time, which can also be proved by comparing the spatial temperature distributions over time obtained from the large- and middle-scale cases [4].

To facilitate the application of experimental-scale studies on hydrate decomposition to field tests, researchers developed a scaling criterion, as outlined in the study by Wang *et al.* [30]. In that study, three devices with inner volumes of 117.80, 5.80 and 0.73 L were employed to assess the scaling criteria in terms of the relationship between gas production ratio and inner volume ratio. The results demonstrated that the ratios of gas production in the DP stage were consistent with the device volume ratios, thus confirming the validity of the scaling criteria. However, for the CP stage, adjustments to the scaling criteria were necessary based on experimental data. Ultimately, the researcher utilized the ratios of research volume and gas production obtained from the large-scale device to predict gas production at a field scale of 50 m × 50 m × 60 m. However, it is challenging to establish a scaling criterion capable of accurately simulating the gas production rate for field-scale predictions through experimental data. This can be attributed to the various limitation

Table 1
Field tests of hydrate production onshore and offshore

	Research area	Year	Method	Duration	Gas production/m^3
Onshore					
1	Mackenzie Delta, Canada [20]	2002	Heating	5 d	~516
2	Mackenzie Delta, Canada [166]	2007	Depressurization	12.5 h	~830
3	Mackenzie Delta, Canada [166]	2008	Depressurization	6 d	~13000
4	North slope of Alaska, USA [167]	2012	CO_2 replacement and depressurization	30 d	~24000
5	Permafrost area of the Qilian Mountains, Qinghai, China [168]	2016	Depressurization	23 d	~1078
Offshore					
1	Nankai Trough, Japan [21]	2013	Depressurization	6 d	~11390
2	Nankai Trough, Japan [169]	2017	Depressurization	12 d	~35000
3	Nankai Trough, Japan [169]	2017	Depressurization	24 d	~200000
4	Shenhu area of SCS, China [22]	2017	Formation fluid extraction	60 d	~309000
5	Shenhu area of SCS, China [170]	2020	Formation fluid extraction	30 d	~861000

degrees of heat transfer and mass transfer between field tests and experimental studies. In addition, differences in heat sources and mass transfer behaviors between field-scale and experimental-scale investigations further complicate the establishment of such criteria, with further details to be discussed in the subsequent section.

3. Natural Gas Hydrate Reservoirs Exploitation by Depressurization

Detailed conditions of typical field-scale production tests are shown in Table 1. International gas hydrate scientific drilling and

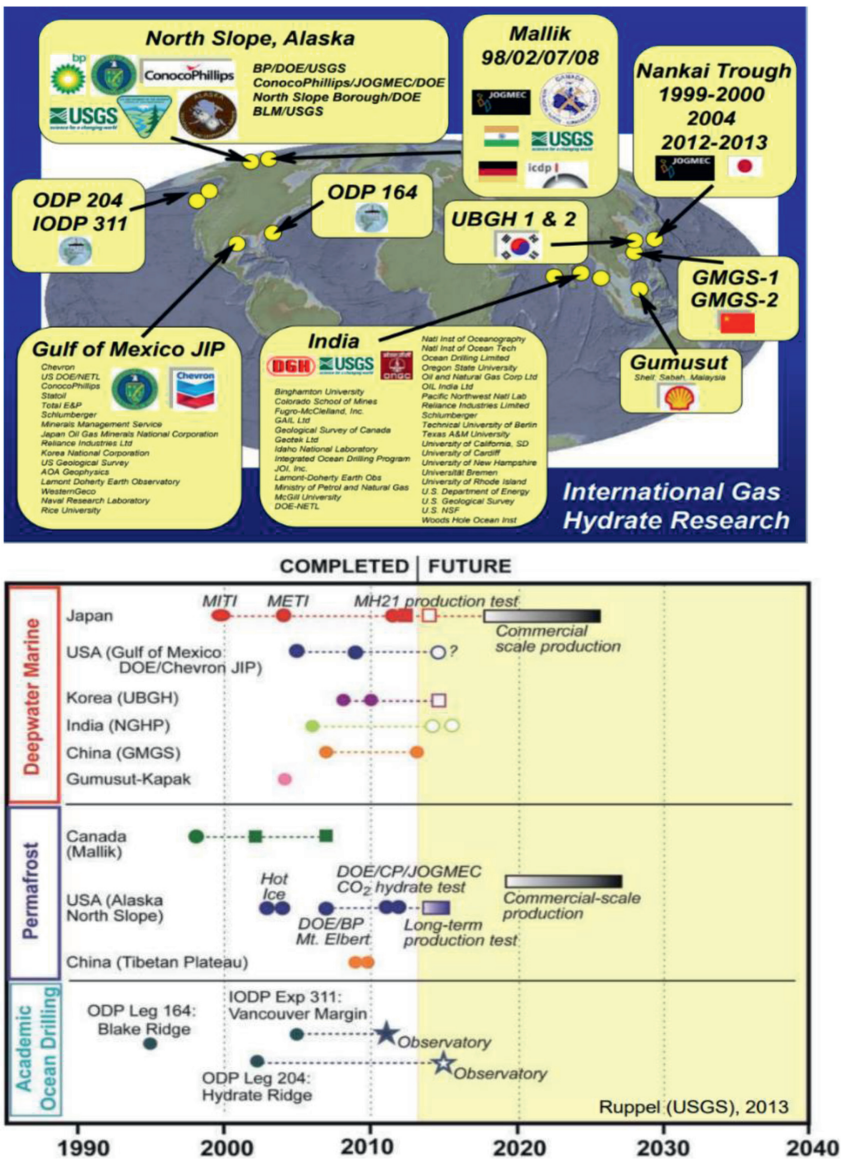

Fig. 6. International gas hydrate scientific drilling and production tests [171].

production tests are depicted in Fig. 6. To date, over 120 sites over the world have found NGH, but only 10 drilling tests were carried out, 5 in permafrost regions (MacKenzie Delta in 2002, 2007, and 2008; Alaska's north slope area in 2012, and Qinghai, China in 2016), and 5 in seafloor (Eastern Nankai Trough, Japan in 2013 and twice in 2017; Shenhu area of the South China Sea, in 2017 and 2020, respectively).

The geological characteristics of hydrate deposits are shown in Table 2. As shown, the natural gas hydrate reservoirs are characterized by large-scale and low permeability, making them challenging to replicate accurately in experimental settings. Consequently, simulating hydrate dissociation within the heat transfer characteristics of the natural environment becomes a complex task. Specifically speaking, in an experimental-scale (including core-, middle-, and large-scale) case, the hydrate decomposition depends on the heat conducted from the device boundaries once the sensible heat within the hydrate deposit has been depleted. For most experimental studies, the temperature of the external environment is constant, ensuring that heat from the boundaries consistently influences the entire hydrate decomposition process. In contrast, the thermodynamic condition of an actual NGHs reservoir is similar to an adiabatic case [155]. The heat comes from the surrounding undecomposed hydrate in the case of a real NGHs reservoir. With the decomposition of NGHs, the ambient temperature gradually decreases until the dissociation progress stops [154].

In addition, real NGHs reservoirs have lower permeability than the most experimental conditions caused by the compression of overburden and surrounding strata. Moreover, in actual NGH reservoirs, grain sediments tend to agglomerate, leading to decreased sediment permeability caused by overburden pressure during gas production. Conversely, in experimental studies, methane hydrate sediment permeability often increases as hydrate dissociation progresses due to the reduction in hydrate saturation. As a result, as seen in Fig. 7, the transfer direction of hydrate decomposition front for actual field-scale tests is opposite to the large-scale experimental studies. In field-scale tests, the NGHs decomposition front initiate from the exploitation well and then extend to the surrounding area [154]. For large-scale experimental studies, as mentioned previously, the hydrate dissociation front aligns with external heat transfer, receding from the reactor boundaries towards the center [49]. This confirms the necessity of NGHs reservoir exploitation tests.

But field-scale tests are characterized by the harsh environment, colossal cost, high risk, and data acquisition technology limitations; Relevant scholars are focusing on numerical simulation [176–179]. Numerical simulations offer the advantage of replicating large-scale, low-permeability environments more easily compared to experiments. Meanwhile, it can reflect the changes in corresponding physical parameters (such as pressure, temperature, permeability, and hydrate saturation) more intuitively in the hydrate decomposition process. However, almost all equations in numerical simulation study were established based on certain assumptions, necessitating more extensive and detailed research in the future.

4. Conclusions and Prospects

From the investigations into hydrate decomposition across different research scales, several key conclusions emerge.

Table 2
Geological characteristics of hydrate deposits

Location	Depth	Reservoir scale	Reservoir property	
			Permeability (md)/porosity	Saturation
Onshore				
Mackenzie Delta, Canada [20]	~890–930 m below the land surface	~40 m thick; ~200 m distance between well	Absolute permeability: 100–1000 md** Initial effective permeability of water: 0.01–10 md Porosity: 0.32–0.38	Hydrate: 50%–80% Water: 20%–50%
Mackenzie Delta, Canada (test in 2007/8) [172]	1070–1110 m below the land surface	~38 m thick; ~200 m distance between well	Absolute permeability: 100–1000 md Initial effective permeability of water: 0.001–1 md Porosity: 0.3–0.4	Hydrate: 50%–95% Water: 50%–5%
Qilian Mountains, Qinghai, China (test in 2011) [173]	133–396 m below the land surface	10–175 m thick	–	Hydrate:13%–86%;
North slope of Alaska, USA [174,175]	~700 m below the surface	10–20 m thick	Absolute permeability: ~1000 md Porosity: 0.03–0.05	Hydrate: ~70% Water: ~25%
Offshore				
Shenhu area of SCS, China [22]	Water depth: 1266 m Mbsf*: 201 m	Three intervals, (1) ~35 m thick; (2) ~15 m thick; (3) ~27 m thick;	Interval (1): 2.9 md/0.35 Interval (2): 1.5 md/0.33 Interval (3): 7.4 md/0.32	(1): Hydrate: 35% (2): Hydrate: 31% (3): Hydrate: 7.8%
Liwan gas reservoirs, north south, China [170]	Water depth: 1310 m Mbsf: 117–196 m	~60 m thick	–	Hydrate: ~70%
Nankai Trough, Japan (test in 2013) [143]	Water depth: 1000 m Mbsf: 300 m	~60 m thick	Absolute permeability: 470–840 md Initial effective permeability of water: 0.01–1 md Porosity: 0.32–0.38	Hydrate: 60%–80%

Note: Mbsf represents “meter below seafloor”. **: 1 md = 0.0009869 μm^2.

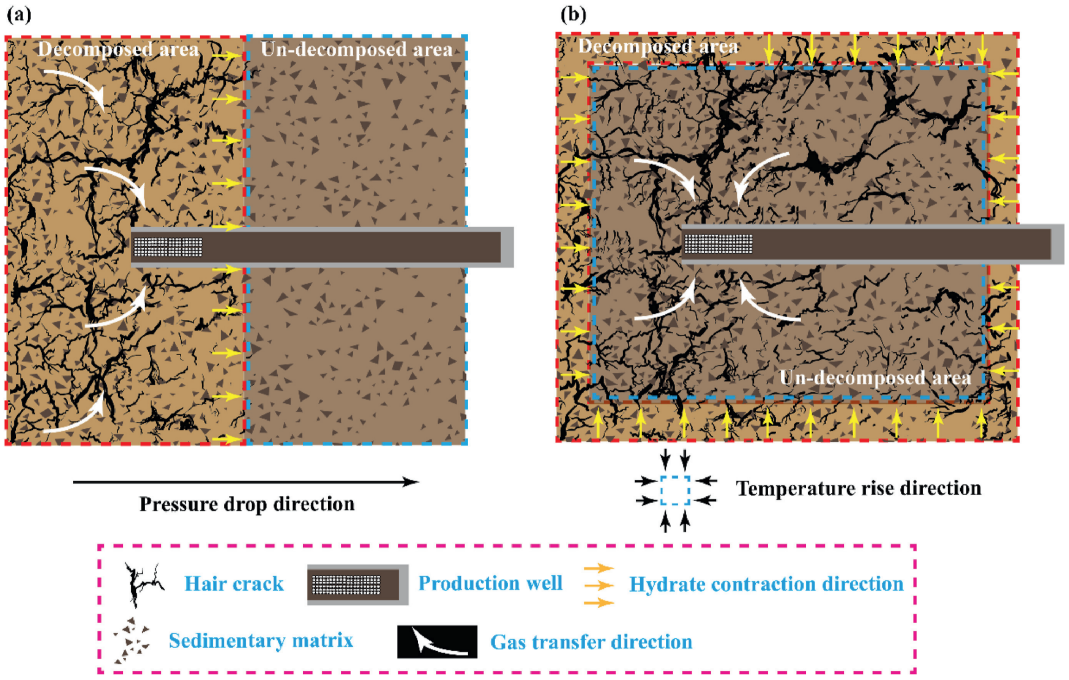

Fig. 7. Comparison between the transfer direction of hydrate decomposition front for actual field-scale tests (a) and experimental-scale studies (b).

(1) Core-scale research: In core-scale studies, the primary rate-limiting factors for hydrate decomposition are intrinsic kinetics and heat transfer. Interestingly, as the research volume increases, the influence of intrinsic kinetics diminishes while that of heat transfer becomes more pronounced.
(2) Large-scale research: In large-scale experiments, heat transfer emerges as the predominant rate-limiting factor for depressurization-induced methane hydrate dissociation.
(3) Middle-scale research: Similar to large-scale experiments, heat transfer takes precedence as the primary rate-limiting factor in middle-scale research. Moreover, the relationship between the contributions of heat conducted from the outside and latent heat in hydrate dissociation resembles that of large-scale experiments under ideal conditions.
(4) Field-scale testing: Field-scale tests reveal that methane hydrate decomposition rates are constrained by both heat and mass transfer. Additionally, field-scale tests present distinct thermodynamic conditions and sediment permeability dynamics during the hydrate decomposition process, resulting in variations in the hydrate decomposition front

As mentioned above, the obtained conclusions under the experimental conditions could differ significantly from the natural hydrate production tests. This can be attributed to the difference between experimental conditions and natural trial production in terms of research scale, thermodynamic condition, and sediment permeability. However, the experimental studies that pay attention to the hydrate sedimentary layer with low permeability and large scale at the same time are very limited. Naturally occurring marine hydrate accumulates and dissociates under axial and confining pressures, which are influenced by water depth and lateral pressure from surrounding strata. The development of core holders capable of applying both axial and confining pressure is crucial to replicate these conditions accurately. The core holder capable of exerting confining and axial pressure is one of the most suitable experimental equipment to account for this condition. In recent years, experimental apparatus that cannot apply confining and axial pressure have been developed from core-scale to large-scale to simulate real exploitation conditions. However, core-scale cases still dominate the core holder focus. Furthermore, there is a lack of experimental studies that simulate adiabatic conditions resembling the natural environment. Therefore, future research should aim to incorporate characteristics such as research scale, thermodynamic conditions, and sediment permeability of actual exploitation conditions simultaneously to obtain data that closely aligns with the real exploitation conditions.

Declaration of Interest

The authors declare that they have no known competing financial interests or personal relationships that could have appeared to influence the work reported in this paper.

Acknowledgements

Financial support received from the National Natural Science Foundation of China (22178379) and the National Key Research and Development Program of China (2021YFC2800902) is gratefully acknowledged.

References

[1] Y.F. Makogon, Natural gas hydrates—A promising source of energy, *J. Nat. Gas Sci. Eng.* 2 (1) (2010) 49–59.
[2] Q.C. Wan, H. Si, B. Li, G. Li, Heat transfer analysis of methane hydrate dissociation by depressurization and thermal stimulation, *Int. J. Heat Mass Tran.* 127 (2018) 206–217.
[3] J.F. Zhao, Z.H. Zhu, Y.C. Song, W.G. Liu, Y. Zhang, D.Y. Wang, Analyzing the process of gas production for natural gas hydrate using depressurization, *Appl. Energy* 142 (2015) 125–134.
[4] X.S. Li, B. Yang, Y. Zhang, G. Li, L.P. Duan, Y. Wang, Z.Y. Chen, N.S. Huang, H.J. Wu, Experimental investigation into gas production from methane hydrate

in sediment by depressurization in a novel pilot-scale hydrate simulator, *Appl. Energy* 93 (2012) 722–732.
[5] M.J. Yang, Z. Fu, Y.C. Zhao, L.L. Jiang, J.F. Zhao, Y.C. Song, Effect of depressurization pressure on methane recovery from hydrate-gas-water bearing sediments, *Fuel* 166 (2016) 419–426.
[6] B. Li, Y.P. Liang, X.S. Li, L. Zhou, A pilot-scale study of gas production from hydrate deposits with two-spot horizontal well system, *Appl. Energy* 176 (2016) 12–21.
[7] J. Lee, Experimental study on the dissociation behavior and productivity of gas hydrate by brine injection scheme in porous rock, *Energy Fuels* 24 (1) (2010) 456–463.
[8] Q. Yuan, C.Y. Sun, X.H. Wang, X.Y. Zeng, X. Yang, B. Liu, Z.W. Ma, Q.P. Li, L. Feng, G.J. Chen, Experimental study of gas production from hydrate dissociation with continuous injection mode using a three-dimensional quiescent reactor, *Fuel* 106 (2013) 417–424.
[9] J.F. Zhao, J.Q. Wang, W.G. Liu, Y.C. Song, Analysis of heat transfer effects on gas production from methane hydrate by thermal stimulation, *Int. J. Heat Mass Tran.* 87 (2015) 145–150.
[10] Z.R. Chong, G.A. Pujar, M.J. Yang, P. Linga, Methane hydrate formation in excess water simulating marine locations and the impact of thermal stimulation on energy recovery, *Appl. Energy* 177 (2016) 409–421.
[11] G.C. Fitzgerald, M.J. Castaldi, Thermal stimulation based methane production from hydrate bearing quartz sediment, *Ind. Eng. Chem. Res.* 52 (19) (2013) 6571–6581.
[12] D.Y. Koh, H. Kang, J.W. Lee, Y. Park, S.J. Kim, J. Lee, J.Y. Lee, H.E. Lee, Energy-efficient natural gas hydrate production using gas exchange, *Appl. Energy* 162 (2016) 114–130.
[13] P.G. Brewer, E.T. Peltzer, P.M. Walz, E.K. Coward, L.A. Stern, S.H. Kirby, J. Pinkston, Deep-sea field test of the CH_4 hydrate to CO_2 hydrate spontaneous conversion hypothesis, *Energy Fuels* 28 (11) (2014) 7061–7069.
[14] O. Ors, C. Sinayuc, An experimental study on the CO_2–CH_4 swap process between gaseous CO_2 and CH_4 hydrate in porous media, *J. Petrol. Sci. Eng.* 119 (2014) 156–162.
[15] Y. Wang, J.C. Feng, X.S. Li, Y. Zhang, G. Li, Analytic modeling and large-scale experimental study of mass and heat transfer during hydrate dissociation in sediment with different dissociation methods, *Energy* 90 (2015) 1931–1948.
[16] Y.P. Liang, X.S. Li, B. Li, Assessment of gas production potential from hydrate reservoir in Qilian Mountain permafrost using five-spot horizontal well system, *Energies* 8 (10) (2015) 10796–10817.
[17] Y. Wang, X.S. Li, G. Li, Y. Zhang, B. Li, J.C. Feng, A three-dimensional study on methane hydrate decomposition with different methods using five-spot well, *Appl. Energy* 112 (2013) 83–92.
[18] Z.R. Chong, Z.Y. Yin, J.H.C. Tan, P. Linga, Experimental investigations on energy recovery from water-saturated hydrate bearing sediments *via* depressurization approach, *Appl. Energy* 204 (2017) 1513–1525.
[19] R.H. Sun, Z. Fan, M.J. Yang, W.X. Pang, Y.P. Li, Y.C. Song, Experimental investigation into the dissociation of methane hydrate near ice-freezing point induced by depressurization and the concomitant metastable phases, *J. Nat. Gas Sci. Eng.* 65 (2019) 125–134.
[20] S. Hancock, T. Collett, S. Dallimore, T. Satoh, T. Inoue, E. Huenges, J. Henninges, B. Weatherill, Overview of thermal-stimulation production-test results for the JAPEX/JNOC/GSC et al. Mallik 5L-38 gas hydrate production research well, in: Scientific Results from the Mallik 2002 Gas Hydrate Production Research Well Program, 2005.
[21] T. Fujii, K. Suzuki, T. Takayama, M. Tamaki, Y. Komatsu, Y. Konno, J. Yoneda, K. Yamamoto, J. Nagao, Geological setting and characterization of a methane hydrate reservoir distributed at the first offshore production test site on the Daini-Atsumi Knoll in the eastern Nankai Trough, Japan, *Mar. Petrol. Geol.* 66 (2015) 310–322.
[22] F.G. Li, Q. Yuan, T.D. Li, L. Zhi, C.Y. Sun, G.J. Chen, A review: Enhanced recovery of natural gas hydrate reservoirs, *Chin. J. Chem. Eng.* 27 (2019) 2062–2073.
[23] Z.Y. Yin, Q.C. Wan, Q. Gao, P. Linga, Effect of pressure drawdown rate on the fluid production behaviour from methane hydrate-bearing sediments, *Appl. Energy* 271 (2020) 115195.
[24] Y. Wang, J.C. Feng, X.S. Li, L. Zhan, X.Y. Li, Pilot-scale experimental evaluation of gas recovery from methane hydrate using cycling-depressurization scheme, *Energy* 160 (2018) 835–844.
[25] Y. Wang, J.C. Feng, X.S. Li, Pilot-scale experimental test on gas production from methane hydrate decomposition using depressurization assisted with heat stimulation below quadruple point, *Int. J. Heat Mass Tran.* 131 (2019) 965–972.
[26] B. Wang, Z. Fan, P.F. Wang, Y. Liu, J.F. Zhao, Y.C. Song, Analysis of depressurization mode on gas recovery from methane hydrate deposits and the concomitant ice generation, *Appl. Energy* 227 (2018) 624–633.
[27] H. Oyama, Y. Konno, K. Suzuki, J. Nagao, Depressurized dissociation of methane-hydrate-bearing natural cores with low permeability, *Chem. Eng. Sci.* 68 (1) (2012) 595–605.
[28] L.G. Tang, X.S. Li, Z.P. Feng, G. Li, S.S. Fan, Control mechanisms for gas hydrate production by depressurization in different scale hydrate reservoirs, *Energy Fuels* 21 (1) (2007) 227–233.
[29] H.C. Kim, P.R. Bishnoi, R.A. Heidemann, S.S.H. Rizvi, Kinetics of methane hydrate decomposition, *Chem. Eng. Sci.* 42 (7) (1987) 1645–1653.
[30] Y. Wang, J.C. Feng, X.S. Li, Y. Zhang, Experimental and modeling analyses of scaling criteria for methane hydrate dissociation in sediment by depressurization, *Appl. Energy* 181 (2016) 299–309.
[31] Z.R. Chong, S.H.B. Yang, P. Babu, P. Linga, X.S. Li, Review of natural gas hydrates as an energy resource: Prospects and challenges, *Appl. Energy* 162 (2016) 1633–1652.
[32] H.O. Kono, S. Narasimhan, F. Song, D.H. Smith, Synthesis of methane gas hydrate in porous sediments and its dissociation by depressurizing, *Powder Technol.* 122 (2–3) (2002) 239–246.
[33] M.Y. Liang, G.J. Chen, C.Y. Sun, L.J. Yan, J. Liu, Q.L. Ma, Experimental and modeling study on decomposition kinetics of methane hydrates in different media, *J. Phys. Chem. B* 109 (40) (2005) 19034–19041.
[34] W.F. Waite, T.J. Kneafsey, W.J. Winters, D.H. Mason, Physical property changes in hydrate-bearing sediment due to depressurization and subsequent repressurization, *J. Geophys. Res.* 113 (B7) (2008) B07102.
[35] D. Katsuki, R. Ohmura, T. Ebinuma, H. Narita, Visual observation of dissociation of methane hydrate crystals in a glass micro model: Production and transfer of methane, *J. Appl. Phys.* 104 (8) (2008) 083514.
[36] X.S. Li, L.H. Wan, G. Li, Experimental investigation into the production behavior of methane hydrate in porous sediment with hot brine stimulation, *Ind. Eng. Chem. Res.* 47 (2008) 9696–9702.
[37] H. Oyama, Y. Konno, Y. Masuda, H. Narita, Dependence of depressurization-induced dissociation of methane hydrate bearing laboratory cores on heat transfer, *Energy Fuels* 23 (10) (2009) 4995–5002.
[38] A. Gupta, G.J. Moridis, T.J. Kneafsey, E.D. Sloan Jr., Modeling pure methane hydrate dissociation using a numerical simulator from a novel combination of X-ray computed tomography and macroscopic data, *Energy Fuels* 23 (12) (2009) 5958–5965.
[39] Y.H. Bai, Q.P. Li, Y. Zhao, X.F. Li, Y. Du, The experimental and numerical studies on gas production from hydrate reservoir by depressurization, *Transp. Porous Medium* 79 (3) (2009) 443–468.
[40] Y.E. Zhou, M.J. Castaldi, T.M. Yegulalp, Experimental investigation of methane gas production from methane hydrate, *Ind. Eng. Chem. Res.* 48 (6) (2009) 3142–3149.
[41] J. Lee, S. Park, W. Sung, An experimental study on the productivity of dissociated gas from gas hydrate by depressurization scheme, *Energy Convers. Manag.* 51 (12) (2010) 2510–2515.
[42] J.Y. Lee, J.C. Santamarina, C. Ruppel, Volume change associated with formation and dissociation of hydrate in sediment, *G-cubed* 11 (3) (2010) Q03007.
[43] K.H. Su, C.Y. Sun, X. Yang, G.J. Chen, S.S. Fan, Experimental investigation of methane hydrate decomposition by depressurizing in porous media with 3-dimension device, *J. Nat. Gas Chem.* 19 (3) (2010) 210–216.
[44] C. Haligva, P. Linga, J.A. Ripmeester, P. Englezos, Recovery of methane from a variable-volume bed of silica sand/hydrate by depressurization, *Energy Fuels* 24 (5) (2010) 2947–2955.
[45] X.S. Li, Y. Wang, G. Li, Y. Zhang, Experimental investigations into gas production behaviors from methane hydrate with different methods in a cubic hydrate simulator, *Energy Fuels* 26 (2) (2012) 1124–1134.
[46] X.S. Li, Y. Zhang, G. Li, Z.Y. Chen, H.J. Wu, Experimental investigation into the production behavior of methane hydrate in porous sediment by depressurization with a novel three-dimensional cubic hydrate simulator, *Energy Fuels* 25 (10) (2011) 4497–4505.
[47] Q.B. Wu, Y.M. Wang, J. Zhan, Effect of rapidly depressurizing and rising temperature on methane hydrate dissociation, *J. Nat. Gas Chem.* 21 (1) (2012) 91–97.
[48] X. Yang, C.Y. Sun, K.H. Su, Q. Yuan, Q.P. Li, G.J. Chen, A three-dimensional study on the formation and dissociation of methane hydrate in porous sediment by depressurization, *Energy Convers. Manag.* 56 (2012) 1–7.
[49] G. Li, B. Li, X.S. Li, Y. Zhang, Y. Wang, Experimental and numerical studies on gas production from methane hydrate in porous media by depressurization in pilot-scale hydrate simulator, *Energy Fuels* 26 (10) (2012) 6300–6310.
[50] S. Falser, S. Uchida, A.C. Palmer, K. Soga, T.S. Tan, Increased gas production from hydrates by combining depressurization with heating of the wellbore, *Energy Fuels* 26 (10) (2012) 6259–6267.
[51] A. Kumar, B. Maini, P.R. Bishnoi, M. Clarke, Investigation of the variation of the surface area of gas hydrates during dissociation by depressurization in porous media, *Energy Fuels* 27 (10) (2013) 5757–5769.
[52] J.Y. Sun, Y.G. Ye, C.L. Liu, J.A. Zhang, Experimental study on gas production from methane hydrate bearing sand by depressurization, *Appl. Mech. Mater.* 310 (2013) 28–32.
[53] S. Falser, A.C. Palmer, K.B. Cheong, T.T. Soon, Temperature increase during the depressurization of partially hydrate-saturated formations within the stability region, *Energy Fuels* 27 (2) (2013) 796–803.
[54] J.F. Zhao, X.Q. Chen, Y.C. Song, Z.H. Zhu, L. Yang, Y.L. Tian, J.Q. Wang, M.J. Yang, Y. Zhang, Experimental study on a novel way of methane hydrates recovery: Combining CO_2 replacement and depressurization, *Energy Proc.* 61 (2014) 75–79.
[55] B. Li, X.S. Li, G. Li, J.C. Feng, Y. Wang, Depressurization induced gas production from hydrate deposits with low gas saturation in a pilot-scale hydrate simulator, *Appl. Energy* 129 (2014) 274–286.
[56] Y. Konno, Y. Jin, K. Shinjou, J. Nagao, Experimental evaluation of the gas recovery factor of methane hydrate in sandy sediment, *RSC Adv.* 4 (93) (2014) 51666–51675.
[57] M. Hyodo, Y.H. Li, J. Yoneda, Y. Nakata, N. Yoshimoto, A. Nishimura, Effects of dissociation on the shear strength and deformation behavior of methane hydrate-bearing sediments, *Mar. Petrol. Geol.* 51 (2014) 52–62.
[58] M. Loh, J.L. Too, S. Falser, P. Linga, B.C. Khoo, A. Palmer, Gas production from methane hydrates in a dual wellbore system, *Energy Fuels* 29 (1) (2015) 35–42.

[59] Y. Zhang, X.S. Li, Z.Y. Chen, X.K. Ruan, N.S. Huang, Methane hydrate dissociation by depressurization in sediments with different hydrate saturations in cubic hydrate simulator, *Energy Proc.* 61 (2014) 990–994.
[60] Y.C. Song, C.X. Cheng, J.F. Zhao, Z.H. Zhu, W.G. Liu, M.J. Yang, K.H. Xue, Evaluation of gas production from methane hydrates using depressurization, thermal stimulation and combined methods, *Appl. Energy* 145 (2015) 265–277.
[61] Y. Zhang, X.S. Li, Z.Y. Chen, Y. Wang, X.K. Ruan, Effect of hydrate saturation on the methane hydrate dissociation by depressurization in sediments in a cubic hydrate simulator, *Ind. Eng. Chem. Res.* 54 (10) (2015) 2627–2637.
[62] J.C. Feng, Y. Wang, X.S. Li, G. Li, Z.Y. Chen, Production behaviors and heat transfer characteristics of methane hydrate dissociation by depressurization in conjunction with warm water stimulation with dual horizontal wells, *Energy* 79 (2015) 315–324.
[63] Y.H. Li, W.G. Liu, Y.M. Zhu, Y.F. Chen, Y.C. Song, Q.P. Li, Mechanical behaviors of permafrost-associated methane hydrate-bearing sediments under different mining methods, *Appl. Energy* 162 (2016) 1627–1632.
[64] J.C. Feng, Y. Wang, X.S. Li, Y. Zhang, Influence of hydrate saturation on methane hydrate dissociation by depressurization in conjunction with warm water stimulation in the silica sand reservoir, *Energy Fuels* 29 (12) (2015) 7875–7884.
[65] S.L. Wang, M.J. Yang, P.F. Wang, Y.C. Zhao, Y.C. Song, *In situ* observation of methane hydrate dissociation under different backpressures, *Energy Fuels* 29 (5) (2015) 3251–3256.
[66] H. Oyama, T. Sato, J. Nagao, Investigation of depressurization with wellbore heating method for Artificial Methane Hydrate Cores, OCEANS 2016, IEEE, Shanghai, China, 2016, pp. 1–6.
[67] L.X. Zhang, J.F. Zhao, H.S. Dong, Y.C. Zhao, Y. Liu, Y. Zhang, Y.C. Song, Magnetic resonance imaging for *in situ* observation of the effect of depressurizing range and rate on methane hydrate dissociation, *Chem. Eng. Sci.* 144 (2016) 135–143.
[68] Y. Wang, J.C. Feng, X.S. Li, Y. Zhang, G. Li, Large scale experimental evaluation to methane hydrate dissociation below quadruple point in sandy sediment, *Appl. Energy* 162 (2016) 372–381.
[69] Y. Wang, J.C. Feng, X.S. Li, Y. Zhang, Z.Y. Chen, Large scale experimental investigation on influences of reservoir temperature and production pressure on gas production from methane hydrate in sandy sediment, *Energy Fuels* 30 (4) (2016) 2760–2770.
[70] D.X. Li, S.R. Ren, L.A. Zhang, Y.X. Liu, Dynamic behavior of hydrate dissociation for gas production *via* depressurization and its influencing factors, *J. Petrol. Sci. Eng.* 146 (2016) 552–560.
[71] J.C. Feng, Y. Wang, X.S. Li, Energy and entropy analyses of hydrate dissociation in different scales of hydrate simulator, *Energy* 102 (2016) 176–186.
[72] J.C. Feng, Y. Wang, X.S. Li, Hydrate dissociation induced by depressurization in conjunction with warm brine stimulation in cubic hydrate simulator with silica sand, *Appl. Energy* 174 (2016) 181–191.
[73] H. Minagawa, T. Ito, S. Kimura, H. Kaneko, S. Noda, N. Tenma, Depressurization and electrical heating of methane hydrate sediment for gas production: laboratory-scale experiments, *J. Nat. Gas Sci. Eng.* 50 (2018) 147–156.
[74] Y.H. Sun, K. Su, S.L. Li, J. Carroll, Y.H. Zhu, Experimental investigation into the dissociation behavior of CH_4–C_2H_6–C_3H_8 hydrates in sandy sediments by depressurization, *Energy Fuels* 32 (2017) 204–213.
[75] B. Wang, H.S. Dong, Y.Z. Liu, X. Lv, Y. Liu, J.F. Zhao, Y.C. Song, Evaluation of thermal stimulation on gas production from depressurized methane hydrate deposits, *Appl. Energy* 227 (2018) 710–718.
[76] Z. Fan, C.M. Sun, Y.M. Kuang, B. Wang, J.F. Zhao, Y.C. Song, MRI analysis for methane hydrate dissociation by depressurization and the concomitant ice generation, *Energy Proc.* 105 (2017) 4763–4768.
[77] Y.R. Jin, S.X. Li, D.Y. Yang, X.X. Jiang, Determination of dissociation front and operational optimization for hydrate development by combining depressurization and hot brine stimulation, *J. Nat. Gas Sci. Eng.* 50 (2018) 215–230.
[78] B. Li, S.D. Liu, Y.P. Liang, Experimental study of methane hydrate dissociation by depressurization and electrical heating, *Energy Proc.* 105 (2017) 5018–5025.
[79] J.C. Feng, Y. Wang, X.S. Li, Large scale experimental evaluation to methane hydrate dissociation below quadruple point by depressurization assisted with heat stimulation, *Energy Proc.* 142 (2017) 4117–4123.
[80] M.J. Yang, Z. Fu, L.L. Jiang, Y.C. Song, Gas recovery from depressurized methane hydrate deposits with different water saturations, *Appl. Energy* 187 (2017) 180–188.
[81] B. Wang, H.S. Dong, Z. Fan, J.F. Zhao, Y.C. Song, Gas production from methane hydrate deposits induced by depressurization in conjunction with thermal stimulation, *Energy Proc.* 105 (2017) 4713–4717.
[82] J.C. Feng, Y. Wang, X.S. Li, Entropy generation analysis of hydrate dissociation by depressurization with horizontal well in different scales of hydrate reservoirs, *Energy* 125 (2017) 62–71.
[83] J.S. Lu, Y.M. Xiong, D.L. Li, X.D. Shen, Q. Wu, D.Q. Liang, Experimental investigation of characteristics of sand production in wellbore during hydrate exploitation by the depressurization method, *Energies* 11 (7) (2018) 1673.
[84] Y. Chen, Y.H. Gao, L.T. Chen, X.R. Wang, K. Liu, B.J. Sun, Experimental investigation of the behavior of methane gas hydrates during depressurization-assisted CO_2 replacement, *J. Nat. Gas Sci. Eng.* 61 (2019) 284–292.
[85] D.L. Li, Q. Wu, Z. Wang, J.S. Lu, D.Q. Liang, X.S. Li, Tri-axial shear tests on hydrate-bearing sediments during hydrate dissociation with depressurization, *Energies* 11 (7) (2018) 1819.
[86] T.T. Luo, Y.H. Li, W.G. Liu, Y.C. Song, Experimental studies on gas production rate of *in situ* hydrate-bearing clay in thermal recovery and depressurization methods, *Energy Proc.* 158 (2019) 5251–5256.
[87] Y. Gao, M.J. Yang, J.N. Zheng, B.B. Chen, Production characteristics of two class water-excess methane hydrate deposits during depressurization, *Fuel* 232 (2018) 99–107.
[88] G. Han, T.H. Kwon, J.Y. Lee, T.J. Kneafsey, Depressurization-induced fines migration in sediments containing methane hydrate: X-ray computed tomography imaging experiments, *J. Geophys. Res.* 123 (4) (2018) 2539–2558.
[89] V.C. Nair, S.K. Prasad, R. Kumar, J.S. Sangwai, Energy recovery from simulated clayey gas hydrate reservoir using depressurization by constant rate gas release, thermal stimulation and their combinations, *Appl. Energy* 225 (2018) 755–768.
[90] Y.P. Liang, S. Liu, W.T. Zhao, B. Li, Q.C. Wan, G. Li, Effects of vertical center well and side well on hydrate exploitation by depressurization and combination method with wellbore heating, *J. Nat. Gas Sci. Eng.* 55 (2018) 154–164.
[91] Y. Gao, Z.Q. Ma, M.J. Yang, Y.C. Song, X. Lv, Dissociation characteristic of remolded methane hydrates deposits from South China Sea using depressurization, *Energy Proc.* 158 (2019) 5355–5360.
[92] L. Zhan, Y. Wang, X.S. Li, Experimental study on characteristics of methane hydrate formation and dissociation in porous medium with different particle sizes using depressurization, *Fuel* 230 (2018) 37–44.
[93] M.J. Yang, J.N. Zheng, Y. Gao, Z.Q. Ma, X. Lv, Y.C. Song, Dissociation characteristics of methane hydrates in South China Sea sediments by depressurization, *Appl. Energy* 243 (2019) 266–273.
[94] T. Lv, X.S. Li, Z.Y. Chen, D. Sun, Y. Zhang, K.F. Yan, J. Cai, Experimental investigation on the production behaviors of methane hydrate in sandy sediments by different depressurization strategies, *Energy Technol.* 6 (12) (2018) 2501–2511.
[95] Z.Y. Liu, M.J. Yang, Y. Liu, Y.C. Song, Q.P. Li, Analyzing the Joule-Thomson effect on wellbore in methane hydrate depressurization with different back pressure, *Energy Proc.* 158 (2019) 5390–5395.
[96] B.B. Chen, H.R. Sun, K.H. Li, D.Y. Wang, M.J. Yang, Experimental investigation of natural gas hydrate production characteristics *via* novel combination modes of depressurization with water flow erosion, *Fuel* 252 (2019) 295–303.
[97] S. Almenningen, P. Fotland, M.A. Fernø, G. Ersland, An experimental investigation of gas-production rates during depressurization of sedimentary methane hydrates, *SPE J.* 24 (2) (2019) 522–530.
[98] Z.F. Sun, S. Jia, Q. Yuan, C.Y. Sun, G.J. Chen, One-dimensional study on gas production characteristics of methane hydrate in clayey sediments using depressurization method, *Fuel* 262 (2020) 116561.
[99] Y. Zhang, T. Wang, X.S. Li, K.F. Yan, Y. Wang, Z.Y. Chen, Decomposition behaviors of methane hydrate in porous media below the ice melting point by depressurization, *Chin. J. Chem. Eng.* 27 (9) (2019) 2207–2212.
[100] Z.Y. Yin, L. Huang, P. Linga, Effect of wellbore design on the production behaviour of methane hydrate-bearing sediments induced by depressurization, *Appl. Energy* 254 (2019) 113635.
[101] M.J. Yang, Z.Q. Ma, Y. Gao, L.L. Jiang, Dissociation characteristics of methane hydrate using depressurization combined with thermal stimulation, *Chin. J. Chem. Eng.* 27 (2019) 2089–2098.
[102] Z.F. Sun, N. Li, J.L. Cui, Q. Yuan, C.Y. Sun, G.J. Chen, A novel method to methane hydrate exploitation efficiency *via* forming impermeable overlying CO_2 cap, *Appl. Energy* 240 (2019) 842–850.
[103] V. Chandrasekharan Nair, P. Gupta, J.S. Sangwai, Natural gas production from a marine clayey hydrate reservoir formed in seawater using depressurization at constant pressure, depressurization by constant rate gas release, thermal stimulation, and their implications for real field applications, *Energy Fuels* 33 (4) (2019) 3108–3122.
[104] S.S. Shu, A.H. Tiwikrama, C.D. Yang, M.J. Lee, Phase equilibrium and dynamic behavior of methane hydrates decomposition *via* depressurization in the presence of a promoter tert butanol, *J. Taiwan Inst. Chem. Eng.* 95 (2019) 119–130.
[105] X. Kou, Y. Wang, X.S. Li, Y. Zhang, Z.Y. Chen, Influence of heat conduction and heat convection on hydrate dissociation by depressurization in a pilot-scale hydrate simulator, *Appl. Energy* 251 (2019) 113405.
[106] L.L. Ren, M. Jiang, L.B. Wang, Y.J. Zhu, Z. Li, C.Y. Sun, G.J. Chen, Gas hydrate exploitation and carbon dioxide sequestration under maintaining the stiffness of hydrate-bearing sediments, *Energy* 194 (2020) 116869.
[107] M.J. Yang, Y. Gao, H. Zhou, B.B. Chen, Y.H. Li, Gas production from different classes of methane hydrate deposits by the depressurization method, *Int. J. Energy Res.* 43 (10) (2019) 5493–5505.
[108] Y.R. Jin, D.Y. Yang, S.X. Li, W.X. Pang, Hydrate dissociation conditioned to depressurization below the quadruple point and salinity addition, *Fuel* 255 (2019) 115758.
[109] Y.F. Wang, L.B. Wang, Y. Li, J.X. Gu, C.Y. Sun, G.J. Chen, X.H. Wang, Q. Yuan, N. Li, Effect of temperature on gas production from hydrate-bearing sediments by using a large 196-L reactor, *Fuel* 275 (2020) 117963.
[110] J.H. Choi, J.S. Lin, S. Dai, L. Lei, Y. Seol, Triaxial compression of hydrate-bearing sediments undergoing hydrate dissociation by depressurization, *Geomech. Energy Environ.* 23 (2020) 100187.

[111] Y. Xie, T. Zheng, J.R. Zhong, Y.J. Zhu, Y.F. Wang, Y. Zhang, R. Li, Q. Yuan, C.Y. Sun, G.J. Chen, Experimental research on self-preservation effect of methane hydrate in porous sediments, *Appl. Energy* 268 (2020) 115008.
[112] A. Heydari, K. Peyvandi, Study of biosurfactant effects on methane recovery from gas hydrate by CO_2 replacement and depressurization, *Fuel* 272 (2020) 117681.
[113] S. Circone, L.A. Stern, S.H. Kirby, The role of water in gas hydrate dissociation, *J. Phys. Chem. B* 108 (18) (2004) 5747–5755.
[114] S.R. Davies, M.S. Selim, E.D. Sloan, P. Bollavaram, D.J. Peters, Hydrate plug dissociation, *AIChE J.* 52 (12) (2006) 4016–4027.
[115] Y.C. Song, L.X. Zhang, Q. Lv, M.J. Yang, Z. Ling, J.F. Zhao, Assessment of gas production from natural gas hydrate using depressurization, thermal stimulation and combined methods, *RSC Adv.* 6 (53) (2016) 47357–47367.
[116] X.W. Guo, L. Xu, B. Wang, L.J. Sun, Y.L. Liu, R.P. Wei, L. Yang, J.F. Zhao, Optimized gas and water production from water-saturated hydrate-bearing sediment through step-wise depressurization combined with thermal stimulation, *Appl. Energy* 276 (2020) 115438.
[117] J.A. He, X.S. Li, Z.Y. Chen, Q.P. Li, Y. Zhang, Y. Wang, C.Y. You, Study on methane hydrate distributions in laboratory samples by electrical resistance characteristics during hydrate formation, *J. Nat. Gas Sci. Eng.* 80 (2020) 103385.
[118] X. Kou, X.S. Li, Y. Wang, Y. Zhang, Z.Y. Chen, Distribution and reformation characteristics of gas hydrate during hydrate dissociation by thermal stimulation and depressurization methods, *Appl. Energy* 277 (2020) 115575.
[119] Y. Lee, C. Deusner, E. Kossel, W. Choi, Y. Seo, M. Haeckel, Influence of CH_4 hydrate exploitation using depressurization and replacement methods on mechanical strength of hydrate-bearing sediment, *Appl. Energy* 277 (2020) 115569.
[120] B. Li, L.L. Chen, Q.C. Wan, X. Han, Y.Q. Wu, Y.J. Luo, Experimental study of frozen gas hydrate decomposition towards gas recovery from permafrost hydrate deposits below freezing point, *Fuel* 280 (2020) 118557.
[121] B. Li, W.N. Wei, Q.C. Wan, K. Peng, L.L. Chen, Numerical investigation into the development performance of gas hydrate by depressurization based on heat transfer and entropy generation analyses, *Entropy* 22 (11) (2020) 1212.
[122] X.Y. Li, X.S. Li, Y. Wang, Y. Zhang, Optimization of the production pressure for hydrate dissociation by depressurization, *Energy Fuels* 34 (2020) 4296–4306.
[123] T.T. Luo, Y.H. Li, B.N. Madhusudhan, X. Sun, Y.C. Song, Deformation behaviors of hydrate-bearing silty sediment induced by depressurization and thermal recovery, *Appl. Energy* 276 (2020) 115468.
[124] X.K. Ruan, X.S. Li, Investigation of the methane hydrate surface area during depressurization-induced dissociation in hydrate-bearing porous media, *Chin. J. Chem. Eng.* 32 (2021) 324–334.
[125] Y.Z. Shao, L.B. Yang, Q. Zhang, S.D. Wang, K.F. Wang, R.Z. Xu, Numerical study on gas production from methane hydrate reservoir by depressurization in a reactor, *Renew. Sustain. Energy Rev.* 134 (2020) 110330.
[126] H.R. Sun, B.B. Chen, G.J. Zhao, Y.C. Zhao, M.J. Yang, Y.C. Song, The enhancement effect of water–gas two-phase flow on depressurization process: Important for gas hydrate production, *Appl. Energy* 276 (2020) 115559.
[127] Y. Kanda, J. Okajima, S. Maruyama, A. Komiya, Visualization of methane hydrate decomposition interface and analyses of decomposition rate and interfacial configuration, *Phys. Fluids* 32 (4) (2020) 047105.
[128] Q.C. Wan, L.L. Chen, B. Li, K. Peng, Y.Q. Wu, Insights into the control mechanism of heat transfer on methane hydrate dissociation *via* depressurization and wellbore heating, *Ind. Eng. Chem. Res.* 59 (22) (2020) 10651–10663.
[129] Q.C. Wan, H. Si, B. Li, Z.Y. Yin, Q. Gao, S. Liu, X. Han, L.L. Chen, Energy recovery enhancement from gas hydrate based on the optimization of thermal stimulation modes and depressurization, *Appl. Energy* 278 (2020) 115612.
[130] Q.C. Wan, H. Si, G. Li, J.C. Feng, B. Li, Heterogeneity properties of methane hydrate formation in a pilot-scale hydrate simulator, *Appl. Energy* 261 (2020) 114325.
[131] Y. Wang, X. Kou, J.C. Feng, X.S. Li, Y. Zhang, Sediment deformation and strain evaluation during methane hydrate dissociation in a novel experimental apparatus, *Appl. Energy* 262 (2020) 114397.
[132] Z.R. Wu, W.G. Liu, J.N. Zheng, Y.H. Li, Effect of methane hydrate dissociation and reformation on the permeability of clayey sediments, *Appl. Energy* 261 (2020) 114479.
[133] J.F. Zhao, Y.L. Liu, X.W. Guo, R.P. Wei, T.B. Yu, L. Xu, L.J. Sun, L. Yang, Gas production behavior from hydrate-bearing fine natural sediments through optimized step-wise depressurization, *Appl. Energy* 260 (2020) 114275.
[134] J. Zhao, J.N. Zheng, S.H. Ma, Y.C. Song, M.J. Yang, Formation and production characteristics of methane hydrates from marine sediments in a core holder, *Appl. Energy* 275 (2020) 115393.
[135] J.N. Zheng, X.R. Wang, Z.Q. Ma, M.J. Yang, Production behaviors of water-saturated methane hydrate deposits during the depressurization with/without thermal water compensation process, *Energy Fuels* 35 (2) (2021) 1638–1647.
[136] C.Y. Sun, G.J. Chen, Methane hydrate dissociation above 0 °C and below 0 °C, *Fluid Phase Equil.* 242 (2) (2006) 123–128.
[137] M. Clarke, P.R. Bishnoi, Determination of the intrinsic rate of ethane gas hydrate decomposition, *Chem. Eng. Sci.* 55 (21) (2000) 4869–4883.
[138] H. Hong, M. Pooladi-Darvish, P. Bishnoi, Analytical modelling of gas production from hydrates in porous media, *J. Can. Petrol. Technol.* 42 (2003) 45–56.
[139] M.B. Kowalsky, G.J. Moridis, Comparison of kinetic and equilibrium reaction models in simulating gas hydrate behavior in porous media, *Energy Convers. Manag.* 48 (6) (2007) 1850–1863.
[140] Z.Y. Yin, Z.R. Chong, H.K. Tan, P. Linga, Review of gas hydrate dissociation kinetic models for energy recovery, *J. Nat. Gas Sci. Eng.* 35 (2016) 1362–1387.
[141] K. Nazridoust, G. Ahmadi, Computational modeling of methane hydrate dissociation in a sandstone core, *Chem. Eng. Sci.* 62 (22) (2007) 6155–6177.
[142] W.Y. Sean, T. Sato, A. Yamasaki, F. Kiyono, CFD and experimental study on methane hydrate dissociation. Part I. Dissociation under water flow, *AIChE J.* 53 (1) (2007) 262–274.
[143] W.Y. Sean, T. Sato, A. Yamasaki, F. Kiyono, CFD and experimental study on methane hydrate dissociation. Part II. General cases, *AIChE. J.* 53 (8) (2007) 2148–2160.
[144] M.S. Selim, E.D. Sloan, Heat and mass transfer during the dissociation of hydrates in porous media, *AIChE J.* 35 (6) (1989) 1049–1052.
[145] S. Gerami, M. Pooladi-Darvish, Predicting gas generation by depressurization of gas hydrates where the sharp-interface assumption is not valid, *J. Petrol. Sci. Eng.* 56 (1–3) (2007) 146–164.
[146] X.F. Sun, K.K. Mohanty, Kinetic simulation of methane hydrate formation and dissociation in porous media, *Chem. Eng. Sci.* 61 (11) (2006) 3476–3495.
[147] W.Q. Chen, R.L. Hartman, Methane hydrate intrinsic dissociation kinetics measured in a microfluidic system by means of in situ Raman spectroscopy, *Energy Fuels* 32 (11) (2018) 11761–11771.
[148] K.H. Su, C.Y. Sun, A. Dandekar, B. Liu, W.Z. Sun, M.C. Cao, N. Li, X.Y. Zhong, X. Q. Guo, Q.L. Ma, L.Y. Yang, G.J. Chen, Experimental investigation of hydrate accumulation distribution in gas seeping system using a large scale three-dimensional simulation device, *Chem. Eng. Sci.* 82 (2012) 246–259.
[149] J.M. Schicks, E. Spangenberg, R. Giese, B. Steinhauer, J. Klump, M. Luzi, New approaches for the production of hydrocarbons from hydrate bearing sediments, *Energies* 4 (1) (2011) 151–172.
[150] X.S. Li, B. Yang, L.P. Duan, G. Li, N.S. Huang, Y. Zhang, Experimental study on gas production from methane hydrate in porous media by SAGD method, *Appl. Energy* 112 (2013) 1233–1240.
[151] X.S. Li, Y. Wang, G. Li, Y. Zhang, Z.Y. Chen, Experimental investigation into methane hydrate decomposition during three-dimensional thermal huff and puff, *Energy Fuels* 25 (4) (2011) 1650–1658.
[152] W.M. Sung, D.G. Huh, B.J. Ryu, H.S. Lee, Development and application of gas hydrate reservoir simulator based on depressurizing mechanism, *Kor. J. Chem. Eng.* 17 (3) (2000) 344–350.
[153] W. Sung, H. Kang, Experimental investigation of production behaviors of methane hydrate saturated in porous rock, *Energy Sources* 25 (8) (2003) 845–856.
[154] C.G. Xu, X.S. Li, Research progress on methane production from natural gas hydrates, *RSC Adv.* 5 (67) (2015) 54672–54699.
[155] Y. Seol, E. Myshakin, Experimental and numerical observations of hydrate reformation during depressurization in a core-scale reactor, *Energy Fuels* 25 (3) (2011) 1099–1110.
[156] G.G. Tsypkin, Mathematical model of the dissociation of gas hydrates coexisting with ice in natural reservoirs, *Fluid Dynam.* 28 (2) (1993) 223–229.
[157] Y. Konno, H. Oyama, J. Nagao, Y. Masuda, M. Kurihara, Numerical analysis of the dissociation experiment of naturally occurring gas hydrate in sediment cores obtained at the eastern Nankai Trough, Japan, *Energy Fuels* 24 (12) (2010) 6353–6358.
[158] V.I. Vasil'ev, V.V. Popov, G.G. Tsypkin, Numerical investigation of the decomposition of gas hydrates coexisting with gas in natural reservoirs, *Fluid Dynam.* 41 (4) (2006) 599–605.
[159] R.Y. Zheng, S.X. Li, Q.P. Li, X.L. Li, Study on the relations between controlling mechanisms and dissociation front of gas hydrate reservoirs, *Appl. Energy* 215 (2018) 405–415.
[160] X.S. Li, C.G. Xu, Y. Zhang, X.K. Ruan, G. Li, Y. Wang, Investigation into gas production from natural gas hydrate: A review, *Appl. Energy* 172 (2016) 286–322.
[161] R.Y. Zheng, S.X. Li, Q.P. Li, Y.M. Hao, Using similarity theory to design natural gas hydrate experimental model, *J. Nat. Gas Sci. Eng.* 22 (2015) 421–427.
[162] X. Sun, N. Nanchary, K.K. Mohanty, 1-D modeling of hydrate depressurization in porous media, Transp, *Porous Medium* 58 (3) (2005) 315–338.
[163] Y. Wang, J.C. Feng, X.S. Li, Y. Zhang, G. Li, Large scale experimental evaluation to methane hydrate dissociation below quadruple point in sandy sediment, *Appl. Energy* 162 (2016) 372–381.
[164] Y. Wang, J.C. Feng, X.S. Li, Y. Zhang, Z.Y. Chen, Fluid flow mechanisms and heat transfer characteristics of gas recovery from gas-saturated and water-saturated hydrate reservoirs, *Int. J. Heat Mass Tran.* 118 (2018) 1115–1127.
[165] V.A. Kamath, Study of Heat Transfer Characteristics during Dissociation of Gas Hydrates in Porous Media, Pittsburgh University, USA, 1984.
[166] M. Kurihara, A. Sato, K. Funatsu, H. Ouchi, K. Yamamoto, M. Numasawa, T. Ebinuma, H. Narita, Y. Masuda, S. Dallimore, F. Wright, D. Ashford, Analysis of production data for 2007/2008 mallik gas hydrate production tests in Canada. Proceedings of the International Oil and Gas Conference and Exhibition in China, 2010.
[167] T. Collett, J. Bahk, M. Frye, D. Goldberg, J. Husebø, C. Koh, M. Malone, C. Shipp, M. Torres, Historical Methane Hydrate Project Review, USGS Publications Warehouse, 70074263 (2013).
[168] J.F. Li, J.L. Ye, X.W. Qin, H.J. Qiu, N.Y. Wu, H.L. Lu, W.W. Xie, J.G. Lu, F. Peng, Z. Q. Xu, C. Lu, Z.G. Kuang, J.G. Wei, Q.Y. Liang, H.F. Lu, B.B. Kou, The first offshore natural gas hydrate production test in South China Sea, *China Geol* 1 (1) (2018) 5–16.
[169] M. Tamaki, T. Fujii, K. Suzuki, Characterization and prediction of the gas hydrate reservoir at the second offshore gas production test site in the eastern Nankai Trough, Japan, *Energies* 10 (10) (2017) 1678.

[170] J.L. Ye, X.W. Qin, W.W. Xie, H.L. Lu, B.J. Ma, H.J. Qiu, J.Q. Liang, J.A. Lu, Z.G. Kuang, C. Lu, Q.Y. Liang, S.P. Wei, Y.J. Yu, C.S. Liu, B. Li, K.X. Shen, H.X. Shi, Q.P. Lu, J. Li, B.B. Kou, G. Song, B. Li, H.E. Zhang, H.F. Lu, C. Ma, Y.F. Dong, H. Bian, The second natural gas hydrate production test in the South China Sea, *China Geol* 3 (2) (2020) 197–209.
[171] T.S. Collett, Gas hydrates: Update on international activities, U.S, *Geol Surv* (2014) 1–77.
[172] K. Qorbani, B. Kvamme, Non-equilibrium simulation of CH_4 production from gas hydrate reservoirs through the depressurization method, *J. Nat. Gas Sci. Eng.* 35 (2016) 1544–1554.
[173] X. Wang, B. Dong, F. Wang, W.Z. Li, Y.C. Song, Pore-scale investigations on the effects of ice formation/melting on methane hydrate dissociation using depressurization, *Int. J. Heat Mass Tran.* 131 (2019) 737–749.
[174] M.W. Lee, T.S. Collett, Pore- and fracture-filling gas hydrate reservoirs in the gulf of Mexico gas hydrate joint industry project leg II green canyon 955 H well, *Mar. Petrol. Geol.* 34 (1) (2012) 62–71.
[175] T. Akaki, S. Kimoto, F. Oka, Dynamic analysis of hydrate-bearing seabed sediments considering methane gas production induced by depressurization, *Jpn. Geotech. Soc. Spec. Publ.* 2 (18) (2016) 676–680.
[176] X.S. Li, B. Yang, G. Li, B. Li, Numerical simulation of gas production from natural gas hydrate using a single horizontal well by depressurization in Qilian Mountain permafrost, *Ind. Eng. Chem. Res.* 51 (11) (2012) 4424–4432.
[177] J.C. Feng, G. Li, X.S. Li, B. Li, Z.Y. Chen, Evolution of hydrate dissociation by warm brine stimulation combined depressurization in the South China Sea, *Energies* 6 (10) (2013) 5402–5425.
[178] J.F. Zhao, C.C. Ye, Y.C. Song, W.G. Liu, C.X. Cheng, Y. Liu, Y. Zhang, D.Y. Wang, X.K. Ruan, Numerical simulation and analysis of water phase effect on methane hydrate dissociation by depressurization, *Ind. Eng. Chem. Res.* 51 (7) (2012) 3108–3118.
[179] X. Sun, T.T. Luo, L. Wang, H.J. Wang, Y.C. Song, Y.H. Li, Numerical simulation of gas recovery from a low-permeability hydrate reservoir by depressurization, *Appl. Energy* 250 (2019) 7–18.